JMEPEG (2016) 25:2245–2254
DOI: 10.1007/s11665-016-2085-5

1059-9495/$19.00

Microstructure and Corrosion Behavior of Hot-Deformed and Cold-Strained High-Mn Steels

A. Grajcar, M. Kciuk, S. Topolska, and A. Płachcińska

(Submitted May 19, 2015; in revised form October 16, 2015; published online April 29, 2016)

The electrochemical corrosion properties of 26Mn-3Si-3Al and 27Mn-4Si-2Al austenitic steels in two different states were studied in 0.1 M H_2SO_4 and 3.5% NaCl using potentiodynamic polarization tests. The effect of cold deformation on the microstructure and corrosion behavior of steels was analyzed. In acid solution, both steels exhibited lower corrosion resistance than in chloride solution independently on the steel state (hot-rolled, cold-worked). Cold deformation decreases the corrosion resistance, though this effect is smaller than the effect of chemical composition related to the combined Al + Si addition. All steels showed the evidence of pitting corrosion. The intensive dissolution of Fe and Mn takes place in the acid medium.

Keywords austenitic steel, corrosion resistance, high-Mn steel, plastic deformation, potentiodynamic polarization

1. Introduction

Conventional Cr-Ni austenitic stainless steels are used as structural materials due to their excellent corrosion resistance and formability. These properties are related to the presence of chromium and nickel as alloying elements (Ref 1-3). However, applications of the Cr-Ni steels are limited in some sectors because of their high cost. For economical considerations, the development of austenitic alloys with manganese and aluminum, which can replace expensive nickel and chromium additions, is an interesting alternative for some non-critical applications.

Since manganese is a relatively cheap alloying element, it can be successfully used to stabilize the austenitic phase. The pure austenite microstructure can be achieved in Fe-Mn alloys containing at least 25% Mn. This content decreases to about 15% Mn when the steel contains approximately 1% C (Ref 3, 4). The similar effect can be obtained in alloys containing increased nitrogen contents. The high-Mn steels are intensively world-wide investigated because of their superior combination of strength, ductility, and crashworthiness (Ref 4, 5). These properties are due to the twinning-induced plasticity (TWIP) or transformation-induced plasticity (TRIP) phenomena resulting in an enhanced work hardening (Ref 5, 6). Their applications include different structural members and elements with a complicated shape used in the crumple zones of cars. In addition to the automotive industry, the high-Mn steels can be used as replacements for traditional Cr-Ni steels for transportation of liquid gases. Unfortunately, these alloys are characterized by poor corrosion resistance because the Mn-alloyed austenite shows totally different corrosion properties than the classical Cr-Ni steels. It was reported that high-Mn steels show the lowest corrosion resistance in solutions of pH about 1 (Ref 6-8). However, there are still no systematic studies in the literature on their potentiodynamic behavior under conditions of plastic deformation as distinct from Cr-Ni stainless steels.

Corrosion behavior of high-manganese austenitic steels depends on their chemical composition and presence of sulfide inclusions. It was found (Ref 9, 10) that the Mn addition decreases the corrosion resistance of steel. The corrosion resistance of high-Mn steels could be improved by the addition of Al, Cr, Cu, and Mo. It is related to the tendency of these elements to form passive films on a steel surface (Ref 7, 10, 11).

The corrosion behavior has been tested mainly for solution-treated alloys so far (Ref 6, 7, 9, 11). It is well known that microstructure and corrosion properties of austenitic steels depend also on a heat treatment applied and plastic deformation. However, the effect of strain on the corrosion behavior has not attracted the significant attention so far. Ghayad et al. (Ref 12) found that cold working increases the corrosion rate because of deformation twins formed upon deformation. The twins represent regions of a different potential from the matrix and this led to the increase in the corrosion current density. They also observed that high-Mn steel corroded more intensively in the presence of some ferrite fraction formed during aging. A result of the plastic deformation can also be the formation of ε or/and α′ martensites. It was reported (Ref 13, 14) that the corrosion progress is accelerated when the amount of the epsilon martensite phase increases. Unfortunately so far, there are no systematic studies on the effects of hot deformation and cold straining on the corrosion resistance of high-Mn steels. In our previous research (Ref 15), we observed that the thermomechanically processed high-Mn steel containing about 25% Mn showed slightly better corrosion resistance than the solution-treated steel. It was concluded that the limited dislocation density produced due to hot deformation has a smaller effect on the corrosion progress than the bimodal distribution of grain size in the solution-treated steel.

In this study, the comparative investigations of the potentiodynamic polarization behavior of two hot-deformed and cold-strained high-Mn steels with different concentrations of aluminum and silicon were carried out. Hence, the combined effects of hot deformation and cold straining are linked to the

A. Grajcar, M. Kciuk, S. Topolska, and **A. Płachcińska**, Institute of Engineering Materials and Biomaterials, Silesian University of Technology, 18a Konarskiego Street, 44-100 Gliwice, Poland. Contact e-mail: adam.grajcar@polsl.pl.

Table 1 Chemical composition of investigated steel grades (wt.%)

Grade	State	C	Mn	Si	Al	S	P	Nb	Ti	N	O	Fe
27Mn-4Si-2Al	T	0.040	27.5	4.18	1.69	0.017	0.004	0.033	0.010	0.0028	0.0006	bal.
26Mn-3Si-3Al	T, CW	0.065	26.0	3.08	2.87	0.013	0.002	0.034	0.010	0.0028	0.0006	bal.

T thermomechanically processed, *CW* cold-worked

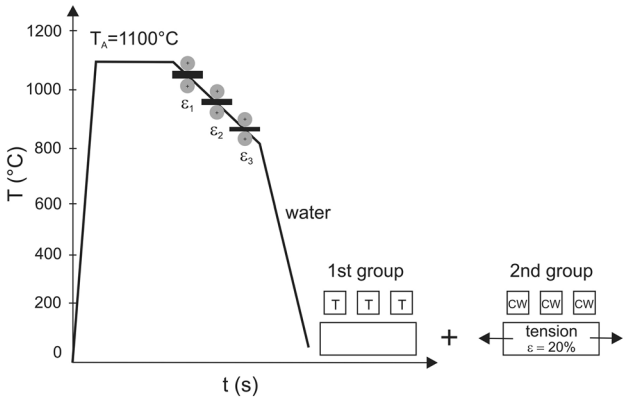

Fig. 1 Hot-rolling and cooling schedule to obtain the 1st group of thermomechanically processed samples (T) and the 2nd group of 20% cold-worked samples (CW) after static tensile test

microstructure and corrosion properties of the investigated steels. There is a lack of the literature data concerning this important topic. This is the novelty of the study.

2. Experimental

2.1 Materials

The chemical composition of the Fe-Mn-Al-Si steels used in the investigation is given in Table 1. Carbon and manganese are major austenite stabilizers. Silicon and aluminum were added for providing solid solution strengthening. Additionally, the microadditions of Nb and Ti were introduced for precipitation strengthening and grain refinement (Ref 16, 17). Steel ingots were prepared by vacuum melting. The next step included hot-forging and rough rolling of samples to a thickness of 4.5 mm. Two groups of specimens were prepared: after thermomechanical rolling and after cold working. The aim was to obtain the steels of the different density of crystallographic defects. The thermomechanical processing consisted of hot rolling of flat samples in 3 passes to a final sheet thickness of approximately 2 mm obtained at the finishing rolling temperature of 850°C (Fig. 1). The detailed conditions of hot rolling are listed in Table 2. Then, the samples were rapidly cooled in water to room temperature. The 1st group of specimens is designated as T. The 2nd group of 26Mn-3Si-3Al steel samples (CW) after thermomechanical rolling was additionally cold deformed in static tensile test to total elongation of 20% within the uniform deformation range.

2.2 Microstructural Investigations

For optical microscopy, the samples were mechanically ground with SiC paper up to 1500 grid, polished with Al_2O_3, and then etched using 5% nital to reveal the microstructure. The investigations were performed using a Zeiss Axio Observer Z1 m optical microscope. Magnifications from 400 to 500 times were applied. The microstructural details were revealed with the SUPRA 25 SEM using back-scattered electrons (BSE) at an accelerating voltage of 20 kV. The EBSD technique using SEM was also applied to assess the microtexture and grain boundaries details of the cold-worked specimens.

X-ray diffraction analysis of the investigated steels in different states (T, CW) was carried out using an x-ray diffractometer (X'Pert PRO). The operating voltage for the x-ray diffractometry was 40 kV and the current value of 30 mA was applied.

2.3 Electrochemical Tests

The corrosion properties of the 27Mn-4Si-2Al and 26Mn-3Si-3Al steels in the different states of treatment (T, CW) were evaluated using the potentiodynamic polarization tests. The corrosion behavior of the thermomechanically processed (T) specimens was compared to the cold-worked (CW) specimens. The electrochemical parameters were evaluated using the average of measurement results of 3 thermomechanically treated and 3 cold-worked specimens.

The electrochemical measurements were performed with the Atlas 0531 Electrochemical Unit potentiostat/galvanostat driven by AtlasCorr05 software. The working surface area of the sample was approximately 0.38 cm^2 and the test media were 0.1 M H_2SO_4 (pH = 1) and 3.5% NaCl (pH = 7) solutions. These solutions are typical corrosive media for the automotive steel sheets, which very often are exposed to hard rain or snow conditions. For instance, car elements are in contact with the NaCl solution during snow removal. On the other hand, the elements suffer from acid rain containing sulfur compounds. The samples were mechanically ground with SiC paper up to 1200 grid, washed in distilled water, and rinsed in acetone prior to tests. All corrosion experiments were conducted using freshly prepared electrolytes. A three-electrode cell was utilized, where the working electrode was the tested steel, the counter and reference electrodes were stainless steel and Ag/AgCl, respectively. The potentiodynamic polarization tests were performed at a scan rate of 0.5 mV/s. Potentiodynamic scan data were collected to determine the electrochemical parameters: corrosion potential E_{corr} and corrosion current density I_{corr}. Solution concentration inside the standard silver electrode (SSE) was 3 M KCl, with a potential of 0.22 V with respect to hydrogen. Electrochemical tests were performed at ambient temperatures and all potentials determined in this work refer to SSE.

The SUPRA 25 scanning electron microscope was used to examine a type of the corrosion attack effects produced on the steel surface after the corrosion tests. Additionally, corrosion damage on cross-sectioned specimens using the Axio Observer Z1 m optical microscope was revealed.

Table 2 Conditions of hot rolling

Pass no.	Deformation temperature (°C)	Sheet thickness before a pass (mm)	Sheet thickness after a pass (mm)	Absolute reduction (mm)	Relative strain (%)
1	1050	4.5	3.4	1.1	25
2	950	3.4	2.5	0.9	25
3	850	2.5	2.0	0.5	20

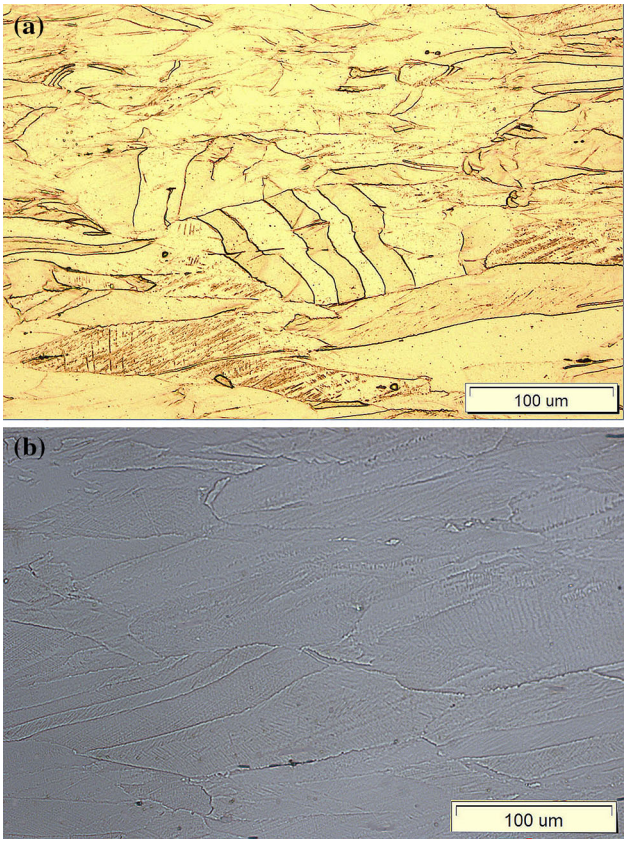

Fig. 2 Austenitic microstructure of the 26Mn-3Si-3Al (a) and 27Mn-4Si-2Al (b) thermomechanically processed steels

3. Results

3.1 Microstructural Investigations

Optical micrographs of the thermomechanically processed steel specimens are shown in Fig. 2(a) and (b). Both micrographs exhibit relatively coarse austenite grains elongated according to the direction of hot rolling. The mean grain size is approximately 80 μm. The microstructures reveal the presence of annealing twins and elongated sulfide inclusions. The micrograph in Fig. 3 shows the 26Mn-3Si-3Al steel specimen after the tensile test performed at room temperature to the 20% strain. The elongated austenite grains and numerous slip bands can be observed. The higher magnification image in Fig. 4 presents some morphological details of the cold-worked specimen. Numerous straight and curved slip lines can be seen. Moreover, the microstructure contains deformation twins.

The additional features of the cold-worked steel can be revealed using the EBSD maps. Figure 5(a) and (b) is the gray scale image quality maps, whereas Fig. 5(c) shows a color-coding map for determination of the crystallographic orientation of individual grains. The grains in Fig. 5(a) are represented by different levels of dark gray what corresponds to the sharpness of the EBSD patters. In turn, the pattern contrast can be an indication of the advancing of dislocation substructure. In general, the darker grains the higher density of structural defects occurs, i.e., grain boundaries, twin boundaries, dislocations, etc. It can be seen that the strain concentrates primarily at grain boundaries. The indirect confirmation of the advanced dislocation substructure is the large amount of low-angle boundaries, i.e., the fraction of the boundaries from 5° to 15° is

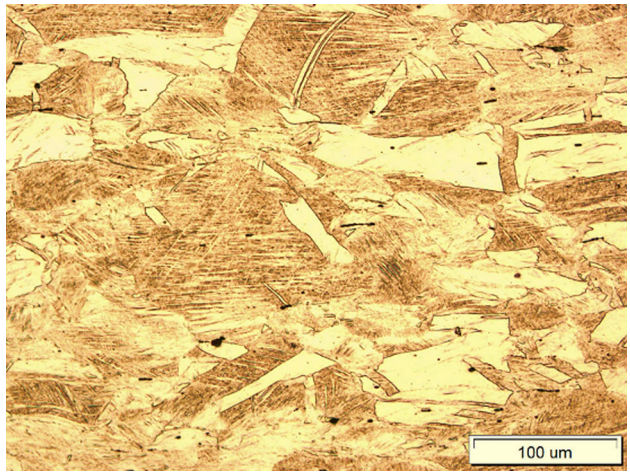

Fig. 3 Austenitic microstructure of the 26Mn-3Si-3Al cold-worked steel

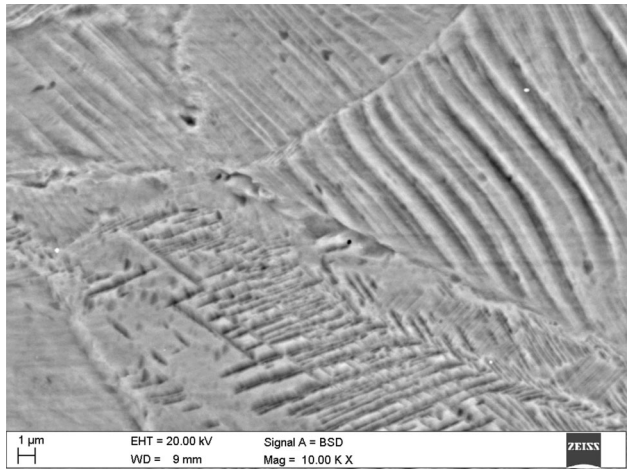

Fig. 4 SEM image of the austenitic microstructure of the 26Mn-3Si-3Al cold-worked steel containing numerous slip lines and deformation twins

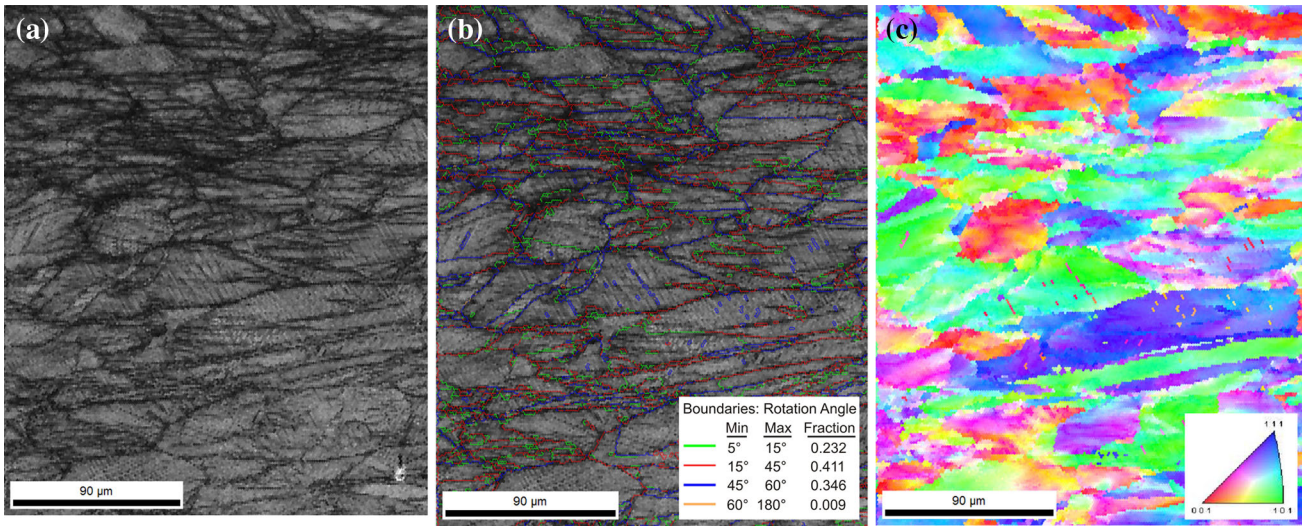

Fig. 5 Image quality map (a), image quality map with misorientations angles (b), and inverse pole figure map (c) of the 26Mn-3Si-3Al steel tensile-strained up to the total elongation of 20%

approximately 23% (Fig. 5b). The remaining part of boundaries are high-angle boundaries. Since twin boundaries are a special type of the high-angle boundaries they can be also easily identified in Fig. 5(b) as parallel straight or curved lines located inside large austenite grains. The inverse pole figure in Fig. 5(c) presents the crystal direction parallel to the specimen normal using color-coding according to the unit triangle. It can be observed that the grains reveal a random crystallographic orientation.

The EBSD analysis and x-ray diffraction patterns obtained from both thermomechanically processed (Fig. 6a and b) and cold-worked (Fig. 6c) specimens confirm that the steels are characterized by the homogeneous austenitic structure.

3.2 Electrochemical Behavior

Average values of corrosion current density I_{corr} and corrosion potential E_{corr} of investigated steels determined by the Tafel slope extrapolation are listed in Table 3. Selected potentiodynamic polarization curves of the thermomechanically processed (T) and cold-worked (CW) specimens obtained in 0.1 M H_2SO_4 and 3.5% NaCl solutions are presented in Fig. 7. The lowest corrosion resistance was obtained in the acid solution, independently on the steel state (thermomechanically treated or cold-deformed). It confirms our earlier results of a weight loss method (Ref 14, 18) and supports the data reported by other authors (Ref 7, 8, 12). Future investigations will also include an impedance technique to confirm these results. The corrosion current density registered in the acid solution was much higher in comparison to chloride solution (Table 3). Kannan et al. (Ref 7) and Lins et al. (Ref 8) reported that high-Mn austenitic steels showed lower corrosion resistance in acid medium than in chloride solution, too.

In 0.1 M H_2SO_4, the polarization behavior of 27Mn-4Si-2Al and 26Mn-3Si-3Al thermomechanically processed specimens was quite similar. The 26Mn-3Si-3Al steel showed the

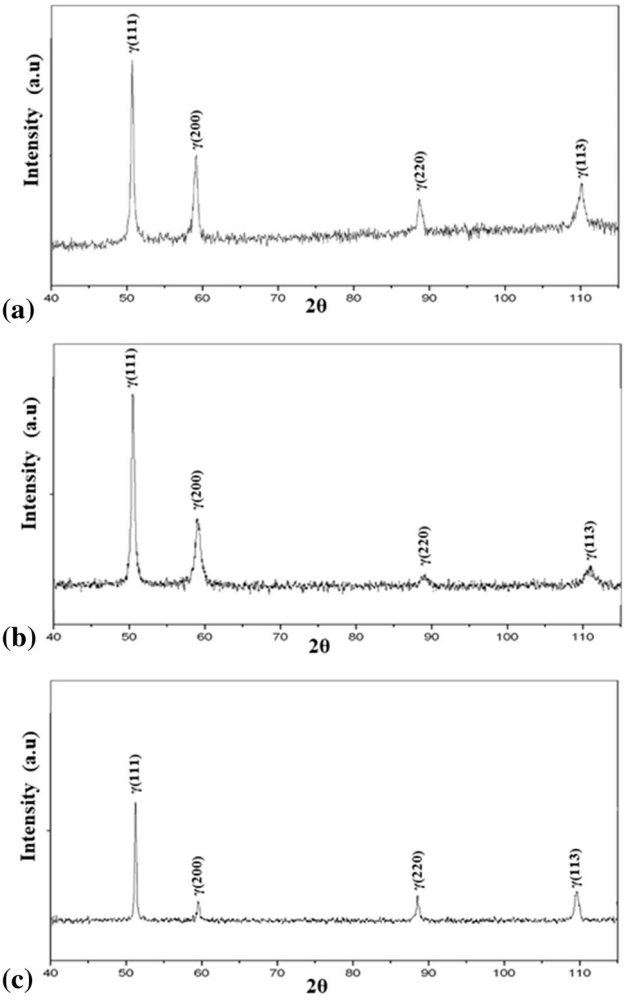

Fig. 6 X-ray diffraction patterns of thermomechanically treated 26Mn-3Si-3Al (a), 27Mn-4Si-2Al (b) steels and cold-worked 26Mn-3Si-3Al steel specimen (c)

Table 3 Average values of electrochemical polarization data of thermomechanically processed and cold-worked steels obtained in the 0.1 M H_2SO_4 and 3.5% NaCl solutions

Material	Type of treatment	Statistics	3.5% NaCl		0.1 M H_2SO_4	
			E_{corr}, mV	I_{corr}, mA/cm^2	E_{corr}, mV	I_{corr}, mA/cm^2
27Mn-4Si-2Al	Thermomechanically processed	Average value	−788	0.090	−584	1.4
		standard deviation	6.5	0.007	6.2	0.2
26Mn-3Si-3Al	Thermomechanically processed	Average value	−785	0.009	−583	1.7
		standard deviation	11.2	0.005	3.3	0.2
26Mn-3Si-3Al	Cold-worked	Average value	−783	0.026	−571	3.7
		standard deviation	16.0	0.002	0.9	0.2

corrosion current density of 1.7 mA/cm^2, whereas it was 1.4 mA/cm^2 for the 27Mn-4Si-2Al steel specimens. The comparison of the polarization behavior of both thermomechanically processed steel specimens in 3.5% NaCl solution indicates that the 26Mn-3Si-3Al steel shows better corrosion resistance. The higher corrosion current density was collected for the steel containing the lower Al content (0.09 mA/cm^2).

In general, the corrosion current density is higher for cold-worked specimens (Table 3). The highest values of the corrosion current density were registered for the cold-deformed 26Mn-3Si-3Al steel specimens examined in the 0.1 M H_2SO_4 solution. Cold deformation increased the corrosion current density to approximately 3.7 mA/cm^2. The corrosion current density measured for the cold-deformed steel specimens of the 26Mn-3Si-3Al steel in acid solution was higher when compared to the both thermomechanically processed specimens. In chloride solution, the cold-deformed steel containing 3% Al showed worse corrosion resistance compared to the thermomechanically rolled samples. The average density of corrosion current registered for cold-worked specimens was about three times higher. It is in good agreement with our earlier results obtained using the weight loss (Ref 14). However, the registered values were lower than those ones measured for the thermomechanically processed steel containing below 2% Al.

The corrosion potential values are similar both in acid (Fig. 7a) and chloride (Fig. 7b) media, independently on the steel state. All specimens polarized in 3.5% NaCl solution show E_{corr} values shifted to less noble potentials (Table 3) when compared to the specimens polarized in 0.1 M H_2SO_4 solution. The E_{corr} shift was about 200 mV toward the cathodic direction. The registered shift between acid and chloride media and the values of corrosion potential cover a range reported for other high-Mn alloys in literature (Ref 7, 8).

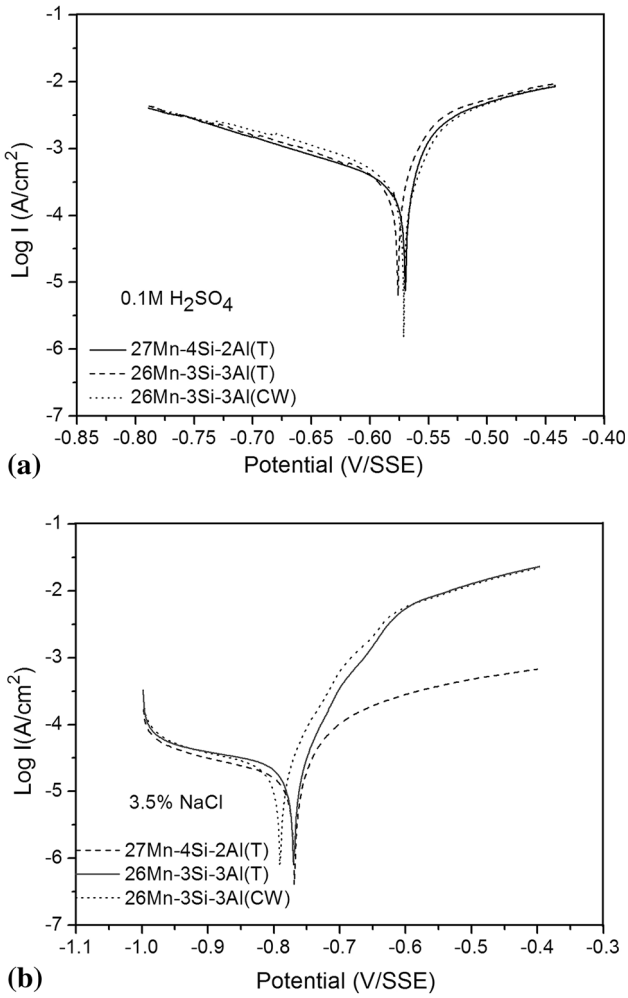

Fig. 7 Selected potentiodynamic polarization curves of thermomechanically treated (T) and cold-worked (CW) steels obtained in 0.1 M H_2SO_4 (a) and 3.5% NaCl (b) solutions

3.3 Corrosion Damage

With the aim to complete the corrosion study, a type of corrosion damage formed during the electrochemical tests was evaluated using microscopic techniques. The SEM micrographs of the thermomechanically processed and cold-worked specimens after the polarization experiments in two different environments are shown in Fig. 8 and 9. Two types of corrosion attack were observed: pitting and uniform corrosion. In acid solution, all specimens showed extensive uniform corrosion in addition to pitting corrosion (Fig. 10a-c). The cold-worked specimens revealed the higher amount of pits, when compared to the thermomechanically processed specimens. Wide and shallow corrosion pits on the specimen surface after corrosion tests in 0.1 M H_2SO_4 were identified. The formation of corrosion pits was presumably associated with the presence of numerous MnS inclusions. Other authors (Ref 8, 9) observed that sulfide inclusions accelerated pitting corrosion processes.

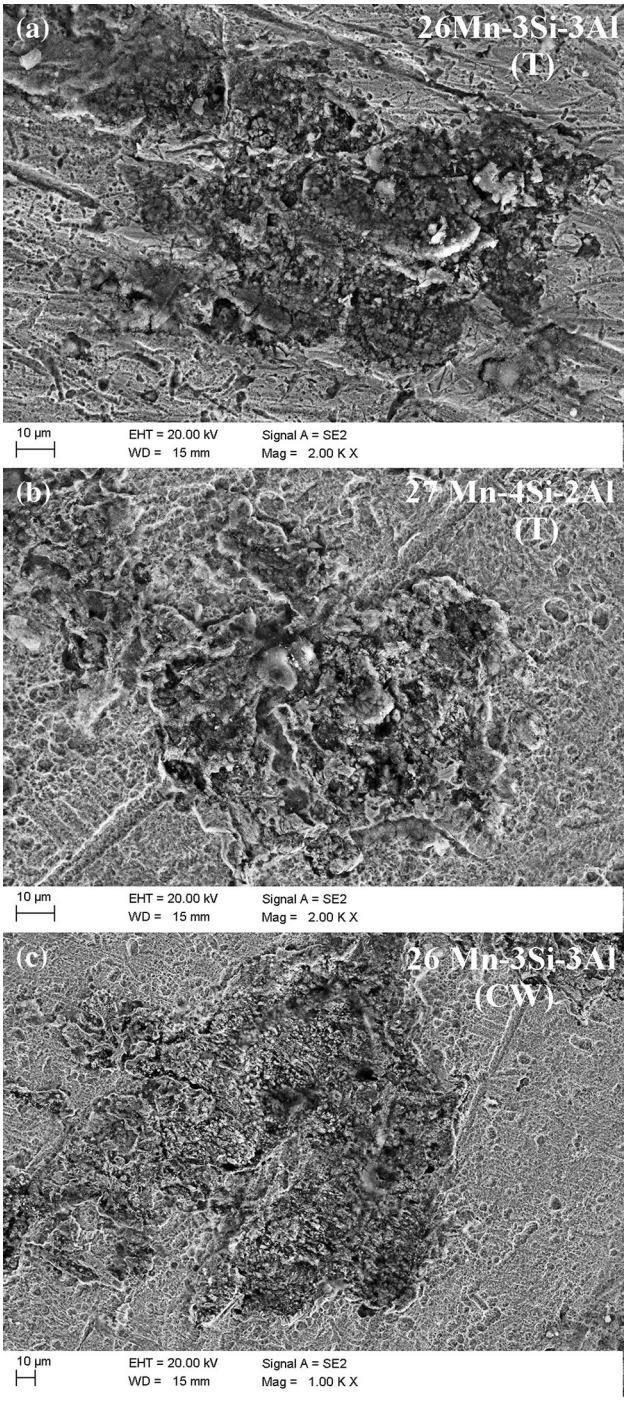

Fig. 8 SEM micrographs of the surface of (a) 26Mn-3Si-3Al, (b) 27Mn-4Si-2Al thermomechanically treated steels and (c) 26Mn-3Si-3Al cold-worked steel potentiodynamically polarized in acid solution

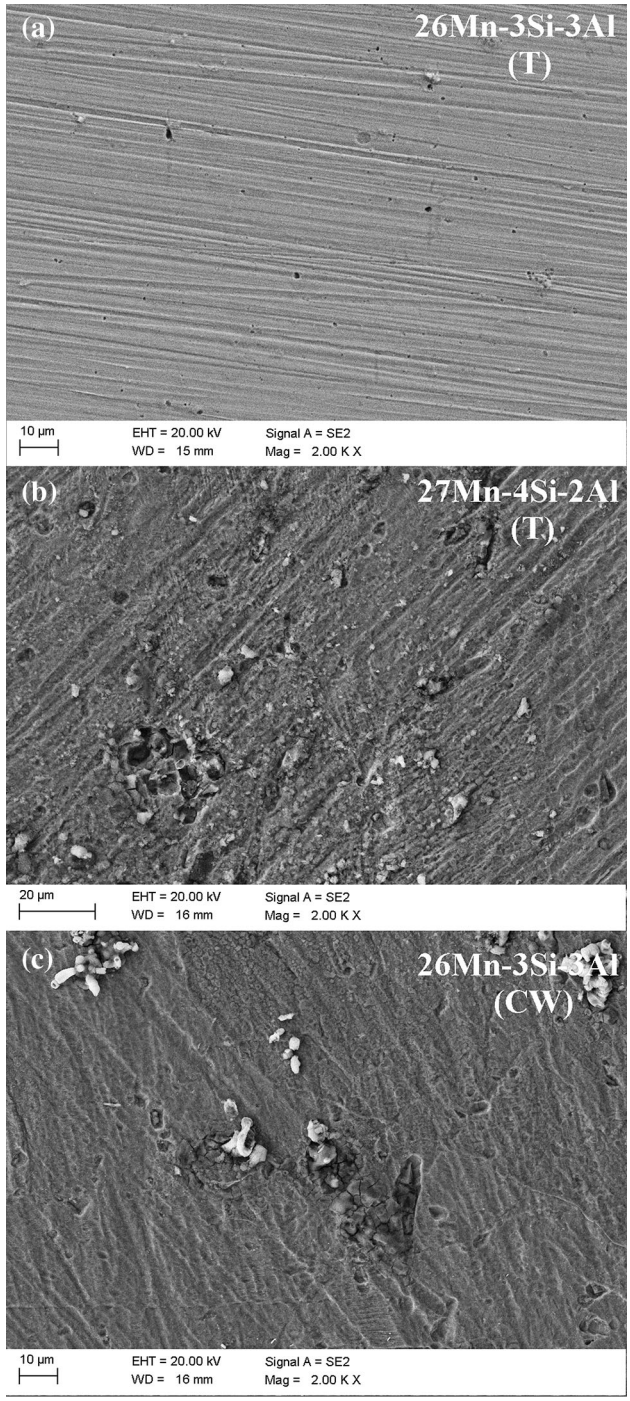

Fig. 9 SEM micrographs of the surface of (a) 26Mn-3Si-3Al, (b) 27Mn-4Si-2Al thermomechanically treated steels, and (c) 26Mn-3Si-3Al cold-worked steel potentiodynamically polarized in chloride solution

In chloride solution, all specimens showed the evidence of pitting corrosion (Fig. 11). It is in good accordance with the data reported by other authors (Ref 7, 8), which identified corrosion pits in different high-manganese steels after polarization tests in chloride solution. The density of corrosion pits and corrosion products at the surface after the corrosion test in the chloride medium is lower when compared to the acid solution. It is reflected by the higher current density of the specimens examined in acid solution (Table 3). Corrosion pits are usually initiated at non-metallic inclusions (Fig. 11).

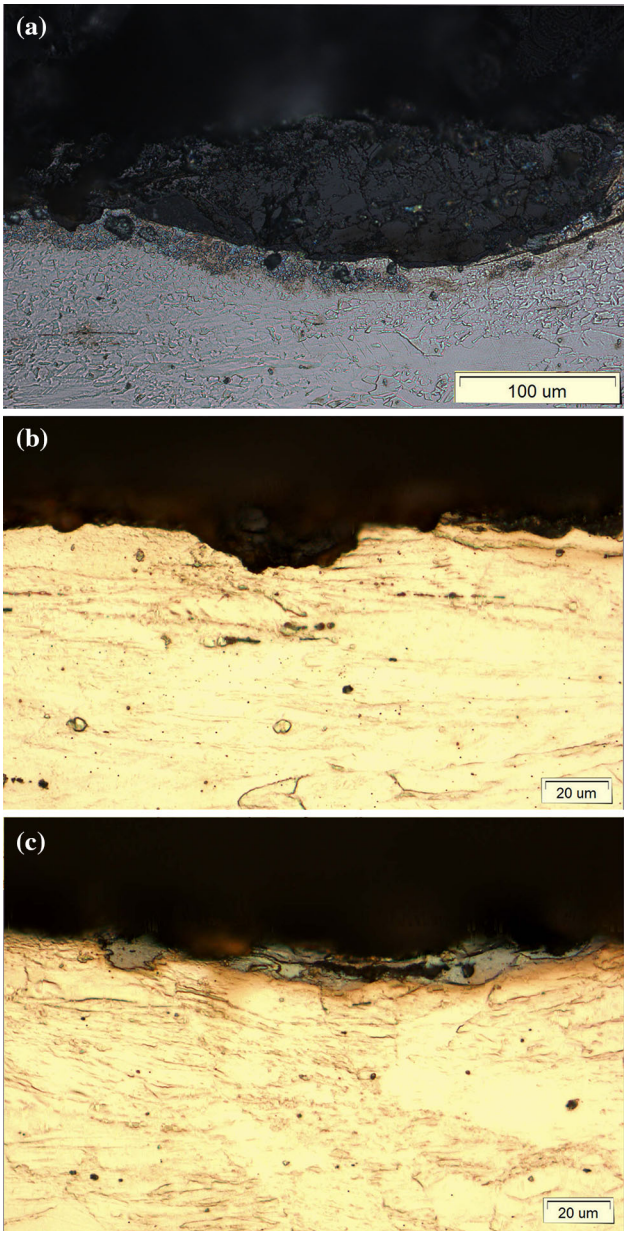

Fig. 10 Optical micrographs of the cross-section of (a) 27Mn-4Si-2Al, (b) 26Mn-3Si-3Al thermomechanically treated steels, and (c) 26Mn-3Si-3Al cold-worked steel potentiodynamically polarized in acid solution

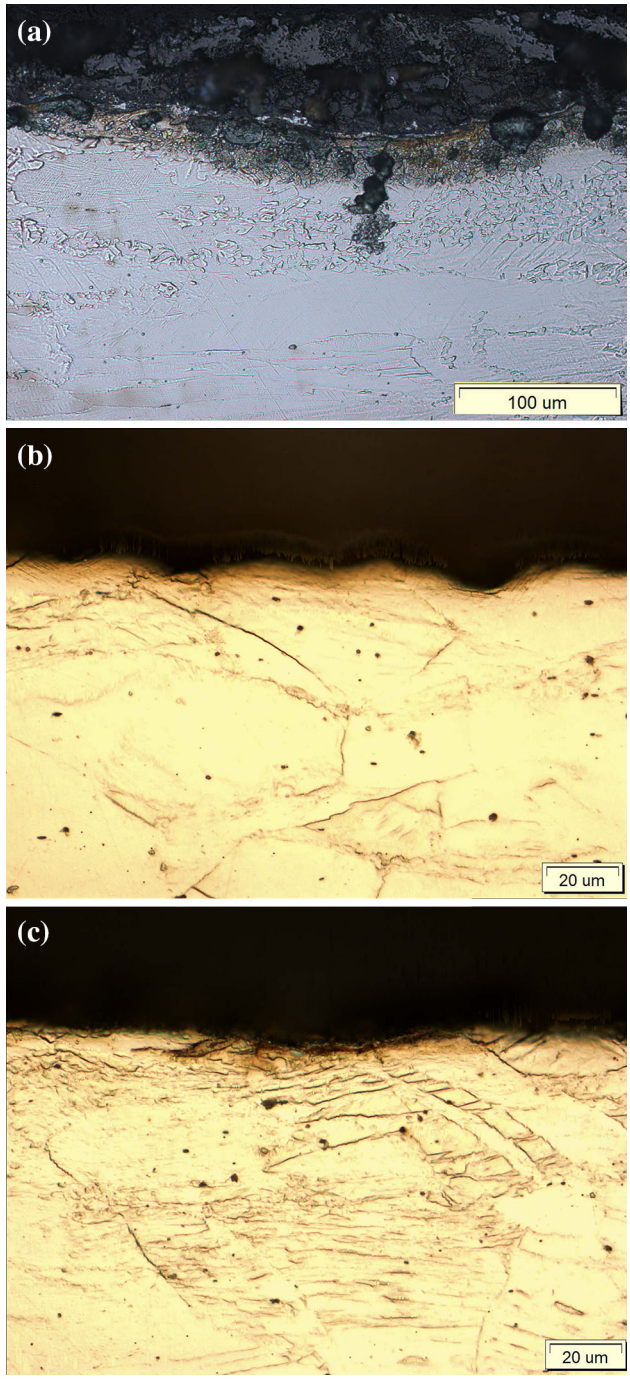

Fig. 11 Optical micrographs of the cross-section of (a) 27Mn-4Si-2Al, (b) 26Mn-3Si-3Al thermomechanically treated steels and (c) 26Mn-3Si-3Al cold-worked steel potentiodynamically polarized in chloride solution

4. Discussion

During the past decade, there have been a number of reports on the corrosion properties of Fe-Mn-Al-Si alloys. Most investigations have focused on the effect of alloying elements on the corrosion resistance. The effect of heat treatment and plastic deformation on the corrosion resistance of high-Mn steels is not well known yet. Since the two investigated steels show a stable austenitic microstructure both after the thermo-mechanical rolling and cold deformation (Fig. 2, 3, 4, and 5, and 6), the corrosion properties should be only affected by the chemical composition of steels and a density of structural defects, which is different for thermomechanically processed and cold-deformed specimens.

4.1 Effect of Chemical Composition

Several studies have shown that the high-manganese steels exhibited lower corrosion resistance in acid solution than in chloride medium. For example, according to Kannan et al. (Ref 7) and Hamada et al. (Ref 19), I_{corr} and E_{corr} values obtained in 3.5% NaCl were 0.028 $mAcm^{-2}$ (−819 mV) and 0.029 $mAcm^{-2}$ (−816 mV), whereas in 0.1 M H_2SO_4, these values are equal to 4.2 $mAcm^{-2}$ (−625 mV) and 3.2 $mAcm^{-2}$ (−608 mV), respectively. In this study, the similar corrosion

current and corrosion potential values were registered (Table 3). Differences in I_{corr} and E_{corr} values are caused by the variation in the chemical composition of different high-Mn steels (various Mn, Al, and Si contents). The results are also affected by the dislocation density and surface quality.

The results obtained in this study confirm above-mentioned behavior, i.e., all specimens show the higher corrosion resistance in 3.5% NaCl solution than in 0.1 M H_2SO_4 medium. It is related to the passivity coefficient of individual alloying elements in the steel. It is well known that Al or Cr additions improve the corrosion resistance of steels while increasing Mn decreases their corrosion resistance (Ref 20-23). It can be explained according to the standard electrode potentials at 25°C. The potential of Al^{3+} (−1.66 V) is more negative to Mn^{2+} (1.51 V) and Fe^{2+} (−0.44 V) (Ref 21). The passivity coefficient of Al is much greater than Mn and Fe (Ref 10). The positive effect of Cr addition to high-Mn steels is reported by Mujica Roncery et al. (Ref 22) whereas the complex Cr + Al addition by Tuan et al. (Ref 23). Alloying with Al improves the passivation ability due to the tendency to formation of stable Al_2O_3 films on the steel surface. The corrosion behavior of steel depends also on pH of corrosion environment. Thus, the mechanism of the corrosion behavior of the investigated steels can be discussed on the basis of the electrochemical potential of the steels and the stability of individual alloying elements according to the Pourbaix diagrams (Ref 20).

The chemical compositions of the investigated steels differ only to a limited extend. The 26Mn-3Si-3Al steel contains a slightly higher Al content and lower Si content in comparison to the 27Mn-4Si-2Al steel (Table 1). Therefore, the polarization behavior of the 27Mn-4Si-2Al and 26Mn-3Si-3Al thermomechanically processed specimens in 0.1 M H_2SO_4 is quite similar. It is related to the fact that in the acid solution (pH = 1), aluminum dissolves as Al^{3+} ions, which prevents the formation of a protective oxide layer (Ref 19). Thus, the high corrosion progress of the examined steels in acid solution is caused by the non-passivating tendency of aluminum in this medium and the enhanced dissolution of iron and manganese (Ref 12, 24).

In 3.5% NaCl solution (pH = 7), aluminum addition improves the corrosion resistance of the steels due to the tendency to formation of the protective Al_2O_3 passive layer on the steel surface. This layer decreases the corrosion current density (Ref 20). Zhang et al. (Ref 24) reported that the Fe-25Mn-5Al steel showed no evidence of passivation. The aluminum content in the investigated steels is limited below 3%. Hence, one should not expect the passivation behavior of the investigated steels. However, the corrosion current density in the steel containing about 3% Al is noticeably smaller in comparison to the steel containing 1.69% Al (Table 3). It means that even such a limited content of aluminum (∼3%) can improve corrosion resistance to a certain degree. Moreover, it is reported (Ref 25) that silicon addition decreases corrosion resistance of steel. Thus, the lower corrosion resistance of the 27Mn-4Si-2Al steel can be also related to its higher silicon concentration.

Manganese addition decreases corrosion resistance of steel, i.e., it dissolves in acid and chloride solutions as Mn^{2+} ions (Ref 8). Its addition is usually accompanied by the reduction of pitting corrosion resistance because of the formation of manganese sulfides (MnS), which act as the initiators of the pitting attack (Ref 9, 26). In our earlier investigations, it was found that the concentration of manganese (at these high-Mn contents) in the steel has no effect on the amount of MnS particles (Ref 27). The amount of non-metallic inclusions depends primarily on the sulfur concentration. Increasing the sulfur concentration causes the increase of MnS quantity. The results showed that the surface fraction of non-metallic inclusions in the 27Mn-4Si-2Al steel with 0.017% S is equal to 0.09%, whereas the 26Mn-3Si-3Al steel containing 0.013% S has a lower fraction of these harmful particles (0.06%). It seems that sulfur can deteriorate the corrosion resistance in this way.

Mn presence displaces E_{corr} toward less noble potential and increases the corrosion current density. The manganese sulfides accelerate the pitting process because the pH decreases in the inner area of the pit and solubilizes MnS inclusions (Eq 1). H_2S dissociates as S^{2-} and HS^- which accelerate the corrosion process (Ref 8).

$$MnS + 2H^+ \rightarrow Mn^{2+} + H_2S. \quad \text{(Eq 1)}$$

In this study, the microscopic observations confirmed that corrosion pits are formed mainly at MnS inclusions.

4.2 Effect of Cold Deformation

Numerous results (Ref 12-14) show that the presence of the second phase after heat treatment (ferrite, ε martensite, and α′ martensite) or as a result of plastic deformation during cold straining (strain induced ε or α′ martensite) increases the corrosion current density. The different phases form a galvanic couple with an austenitic matrix, which accelerate the corrosion rate. In this study, the steels retain the pure austenitic microstructure upon cold straining. Consequently, the lower corrosion resistance of cold-deformed steel specimens (Table 3) has to be related to other factors, i.e., a density of structural defects. The electrochemical results show that in the 0.1 M H_2SO_4 solution, cold deformation of steel has significant effect on its corrosion resistance. In comparison to the thermomechanically processed specimens, the cold deformed 26Mn-3Si-3Al steel specimens are characterized by the lower corrosion resistance. The corrosion current density of the steel containing 3% Al is approximately twice higher after cold straining (Table 3). The SEM and optical micrographs confirm that the amount of corrosion pits in cold-deformed steel specimens is higher than in the thermomechanically processed steels. It is due to the increased dislocation density and numerous twins after cold working (Fig. 3, 4, and 5). The grain boundaries are particularly susceptible to the pit nucleation (Ref 28). Moreover, the high amount of deformation twins present in the microstructure of the cold-deformed steel contributes to the reduction of its corrosion resistance due to the differences in the potential between the matrix and twins, which create local electrochemical corrosion cells (Ref 6, 12).

The corrosion current density of the cold-worked 26Mn-3Si-3Al steel in chloride solution is above three times higher in comparison to the thermomechanically treated specimens (Table 3). However, it is interesting that the current values of the cold-strained 26Mn-3Si-3Al steel are lower when compared to the hot-rolled steel containing a lower Al content. Therefore, the relative effect of cold working is smaller than the combined effects of the decrease of Al addition and the increase of Si content in the 27Mn-4Si-2Al steel. It means that the deterioration of the corrosion resistance is more related to the chemical composition of high-Mn steels than to the effect of cold

deformation. The beneficial effect of the increase of the Al addition from 1.7% to approximately 3% can be noticed.

5. Conclusions

The comparative study of the effects of various Al + Si additions and the different dislocation density in hot-rolled and cold-strained high-Mn steels allow to draw the following conclusions:

1. The 26Mn-3Si-3Al and 27Mn-4Si-2Al austenitic steels are characterized by the lowest corrosion resistance in the 0.1 M H_2SO_4 solution, independently on their thermomechanically treated or cold-strained state. It is attributed to the non-passivating tendency of aluminum in this media in addition to the intensive manganese and iron dissolution. Microscopic observations confirm the presence of pitting and uniform corrosion.
2. Pitting is the major corrosion type in the chloride solution. Wide and shallow corrosion pits located usually at numerous non-metallic inclusions were identified. The corrosion potential values for the chloride medium are −785 mV and about −580 mV for the acid solution independently on the chemical composition and deformation state.
3. Cold deformation accelerates the corrosion progress due to numerous slip bands and deformation twins formed in the austenite. The cold-strained steel samples show the lower corrosion resistance in the acid solution in comparison to the thermomechanically treated steels containing a smaller number of structural defects.
4. The cold-strained steel containing the higher Al (∼3%) content and smaller Si (∼3%) content shows better corrosion resistance in the chloride solution in comparison to the thermomechanically processed 27Mn-4Si-2Al steel. It means that the corrosion behavior of the investigated high-Mn steels is relatively stronger affected by the chemical composition than the cold deformation effects.

Acknowledgment

This work was financially supported with statutory funds of Faculty of Mechanical Engineering of Silesian University of Technology in 2015.

References

1. A.F. Padilha, I.F. Machado, and R.L. Plaut, Microstructures and Mechanical Properties of Fe–15%Cr–15%Ni Austenitic Stainless Steels Containing Different Levels of Niobium Additions Submitted to Various Processing Stages, *J. Mater. Proc. Tech.*, 2005, **170**(1-2), p 89–96
2. M.A.M. Ibrahim, S.S. Abd El Rehim, and M.M. Hamza, Corrosion Behavior of Some Austenitic Stainless Steels in Chloride Environments, *Mater. Chem. Phys.*, 2009, **115**(1), p 80–85
3. Z.H. Jin, H.H. Ge, W.W. Lin, Y.W. Zong, S.J. Liu, and J.M. Shi, Corrosion Behaviour of 316L Stainless Steel and Anti-Corrosion Materials in a High Acidified Chloride Solution, *Appl. Surf. Sci.*, 2014, **322**, p 47–56
4. G. Frommeyer, U. Brüx, and P. Neumann, Supra-Ductile and High-Strength Manganese-TRIP/TWIP Steels for High Energy Absorption Purposes, *ISIJ Int.*, 2003, **43**(3), p 438–446
5. M. Eskandari, A. Zarei-Hanzaki, A.R. Kamali, M.A. Mohtadi-Bonab, and J.A. Szpunar, Strain Hardening During Hot Compression Through Planar Dislocation and Twin-Like Structure in a Low-Density High-Mn Steel, *J. Mater. Eng. Perform.*, 2014, **23**(10), p 3567–3576
6. S. Lasek and E. Mazancova, Influence of Thermal Treatment on Structure and Corrosion Properties of High Manganese TRIPLEX Steels, *Metalurgija*, 2013, **52**(4), p 441–444
7. M.B. Kannan, R.K.S. Raman, and S. Khoddam, Comparative Studies on the Corrosion Properties of a Fe-Mn-Al-Si Steel and an Interstitial-Free Steel, *Corros. Sci.*, 2008, **50**(10), p 2879–2884
8. V.F.C. Lins, M.A. Freitas, and E.M.P. e Silva, Corrosion Resistance Study of Fe–Mn–Al–C Alloys Using Immersion and Potentiostatic Tests, *Appl. Surf. Sci.*, 2005, **250**(1–4), p 124–134
9. I.J. Park, S.M. Lee, M. Kang, S. Lee, and Y.K. Lee, Pitting Corrosion Behavior in Advanced High Strength Steels, *J. Alloy. Compd.*, 2015, **619**, p 205–210
10. Y.S. Zhang, X.M. Zhua, and S.H. Zhong, Effect of Alloying Elements on the Electrochemical Polarization Behavior and Passive Film of Fe–Mn Base Alloys in Various Aqueous Solutions, *Corros. Sci.*, 2004, **46**(4), p 853–876
11. T. Dieudonné, L. Marchetti, M. Wery, F. Miserque, M. Tabarant, J. Chêne, C. Allely, P. Cugy, and C.P. Scott, Role of Copper and Aluminum on the Corrosion Behavior of Austenitic Fe–Mn–C TWIP Steels in Aqueous Solutions and the Related Hydrogen Absorption, *Corros. Sci.*, 2014, **83**, p 234–244
12. I.M. Ghayad, A.S. Hamada, N.N. Girgis, and W.A. Ghanem, Effect of Cold Working on the Aging and Corrosion Behaviour of Fe-Mn-Al Stainless Steel, *Steel Grips*, 2006, **4**, p 133–137
13. Y.S. Chun, J.S. Kim, K.T. Park, Y.K. Lee, and C.S. Lee, Role of ε Martensite in Tensile Properties and Hydrogen Degradation of High-Mn Steels, *Mater. Sci. Eng. A*, 2012, **533**, p 87–95
14. A. Grajcar, W. Krukiewicz, and S. Kołodziej, Corrosion Behaviour of Plastically Deformed High-Mn Austenitic Steels, *J. Achiev. Mater. Manuf. Eng.*, 2010, **43**(1), p 228–235
15. A. Grajcar, A. Płachcińska, S. Topolska, and M. Kciuk, Effect of Thermomechanical Treatment on the Corrosion Behavior of Si and Al-Containing High-Mn Austenitic Steel with Nb and Ti Microaddition, *Mater. Tehnol.*, 2015, **49**, p 889–894
16. A. Grajcar, M. Opiela, and G. Fojt-Dymara, The Influence of Hot-Working Conditions on a Structure of High-Manganese Steel, *Arch. Civ. Mech. Eng.*, 2009, **9**(3), p 49–58
17. L.A. Dobrzański, A. Grajcar, and W. Borek, Microstructure Evolution of C-Mn-Si-Al-Nb High-Manganese Steel During the Thermomechanical Processing, *Mater. Sci. Forum*, 2010, **638–642**, p 3224–3229
18. A. Grajcar, S. Kołodziej, and W. Krukiewicz, Corrosion Resistance of High-Mn Austenitic Steels for the Automotive Industry, *Arch. Mater. Sci. Eng*, 2010, **41**(2), p 77–84
19. A.S. Hamada and L.P. Karjalainen, Corrosion Behaviour of High-Mn TWIP Steels with Electroless Ni-P Coating, *Open Corros. J.*, 2010, **3**, p 1–6
20. N. Takeno, *Atlas of Eh-pH Diagrams*, National Institute of Advanced Science and Technology, Tokyo, 2005
21. K.J. Park and H.S. Kwon, Effects of Mn on the Localized Corrosion Behavior of Fe–18Cr Alloys, *Electrochim. Acta*, 2010, **55**(9), p 3421–3427
22. L. Mujica Roncery, S. Weber, and W. Theisen, Development of Mn-Cr-(C-N) Corrosion Resistant Twinning Induced Plasticity Steels: Thermodynamic and Diffusion Calculations, Production, and Characterization, *Metall. Mater. Trans. A*, 2010, **41**(10), p 2471–2479
23. Y.H. Tuan, C.S. Wang, C.Y. Tsai, C.G. Chao, and T.F. Liu, Corrosion Behaviors of Austenitic Fe-30Mn-7Al-xCr-1C Alloys in 3.5% NaCl Solution, *Mater. Chem. Phys.*, 2009, **114**(2–3), p 595–598

24. Y.S. Zhang and X.M. Zhu, Electrochemical Polarization and Passive Film Analysis of Austenitic Fe-Mn-Al Steels in Aqueous Solutions, *Corros. Sci.*, 1999, **41**(9), p 1817–1833
25. S. Suzuki, E. Matsubara, T. Komatsu, Y. Okamoto, K. Kanie, A. Muramatsu, H. Konishi, J. Mizuki, and Y. Waseda, Ex-Situ and In-Situ X-Ray Diffractions of Corrosion Products Freshly Formed on the Surface of an Iron-Silicon Alloy, *Corros. Sci.*, 2007, **49**(3), p 1081–1096
26. A. Pardo, M.C. Merino, A.E. Coy, F. Viejo, R. Arrabal, and E. Matykina, Pitting Corrosion Behavior of Austenitic Stainless Steels: Combining Effects of Mn and Mo Additions, *Corros. Sci.*, 2008, **50**(6), p 1796–1806
27. A. Grajcar, U. Galisz, and L. Bulkowski, Non-metallic Inclusions in High Manganese Austenitic Alloys, *Arch. Mater. Sci. Eng.*, 2011, **50**(1), p 21–30
28. A. Di Schino, M. Barteri, and J.M. Kenny, Grain Size Dependence of Mechanical, Corrosion and Tribological Properties of High Nitrogen Stainless Steels, *J. Mater. Sci.*, 2003, **38**(15), p 3257–3262